

## Quark condensates and the deconfinement transition

---

**Christian S. Fischer**<sup>\*†</sup>

*Institute for Nuclear Physics, Darmstadt University of Technology,  
Schlossgartenstraße 9, 64289 Darmstadt, Germany  
GSI Helmholtzzentrum für Schwerionenforschung GmbH,  
Planckstraße 1, 64291 Darmstadt, Germany.  
E-mail: christian.fischer@physik.tu-darmstadt.de*

**Jens A. Mueller**

*Institute for Nuclear Physics, Darmstadt University of Technology,  
Schlossgartenstraße 9, 64289 Darmstadt, Germany  
E-mail: jens.mueller@physik.tu-darmstadt.de*

In this talk we present results on the chiral and the deconfinement transition of quenched QCD from Dyson-Schwinger equations. We determine the ordinary quark condensate signaling the chiral transition and the dual quark condensate signaling the deconfinement transition from the Landau gauge quark propagator evaluated at generalized boundary conditions. We find only slightly different transition temperatures at finite quark masses, whereas the transition temperatures coincide in the chiral limit.

*5th International Workshop on Critical Point and Onset of Deconfinement - CPOD 2009,  
June 08 - 12 2009  
Brookhaven National Laboratory, Long Island, New York, USA*

---

<sup>\*</sup>Speaker.

<sup>†</sup>This work has been supported by the Helmholtz Young Investigator Grant VH-NG-332 and by the Helmholtz Alliance HA216-TUD/EMMI.

## 1. Introduction

The QCD phase diagram is a matter of intense investigation from both, theory and experiment. Some of the pressing open questions discussed at this conference are the presence or absence of a critical point [1], the possibility of a confined chirally symmetric ('quarkyonic') phase [2] and the (non-)coincidence of the chiral and the deconfinement transition at zero chemical potential [3, 4]. Answers to these questions certainly require nonperturbative approaches to QCD. On the other hand, the considerable complexity of these questions suggests that one approach alone is hardly capable to provide all answers. Instead it seems promising to combine the various available methods in order to balance their respective strengths and weaknesses.

Lattice Monte-Carlo simulations are well behaved at zero or imaginary chemical potential, but encounter the notorious sign problem when it comes to real chemical potential. One approach to overcome this problem, extrapolation from zero chemical potential by Taylor-expansion methods (see e.g. [5]), has been questioned recently on the basis of the failure of corresponding extrapolations in model calculations [6]. These models, notably the Polyakov-NJL model and the Polyakov-quark-meson model (see e.g. [7, 8, 9] and refs. therein) have been employed frequently to explore the details of the QCD phase diagram at zero and finite chemical potential. Their success is demonstrated e.g. by the quantitative reproduction of the lattice equation of state at zero chemical potential. Furthermore they serve as a formidable qualitative playground to explore scenarios for the details of the interplay between the chiral and the deconfinement transition. Nevertheless, it is hard to see how the various model parameters can be constrained enough to arrive at quantitative predictions as e.g. the location of a possible critical point [10].

A third class of approaches are functional methods involving the renormalization group equations [11] and/or Dyson-Schwinger equations [12, 13] of QCD. In the past years much progress has been made in extending these methods to finite temperature and/or chemical potential, see e.g. [14, 12, 15, 16, 17, 18, 19, 20]. Most of the earlier works involving functional methods concentrated on the chiral aspects of the QCD transition. Recently, methods became available that also take into account the deconfining aspect [14, 16, 18, 19, 20]. In this talk we report on results from one particular method that extracts the deconfinement transition temperature from the properties of the quark propagator at generalized boundary conditions. This method has been introduced originally within the lattice framework [21, 22] and adapted to functional methods in [18, 19, 20]. The quantity signaling the deconfinement transition is the dual quark condensate (or 'dressed Polyakov loop'). It transforms under center transformations exactly like the ordinary Polyakov loop and is therefore an order parameter in the limit of infinitely heavy quarks. This quantity is furthermore interesting from a formal perspective since it relates both the chiral and the deconfinement transition to the spectral properties of the Dirac operator [21, 23].

In the following we first recall the defining equations for the ordinary and the dual quark condensate, then summarize the truncation scheme used in our DSE calculations before we discuss our results for the chiral and deconfinement phase transition.

## 2. The dual quark condensate

Consider the quark propagator  $S(\vec{p}, \omega_p)$  at finite temperature given by the tensor decomposition

$$S(\vec{p}, \omega_p) = [i\gamma_4 \omega_p C(\vec{p}, \omega_p) + i\gamma_i p_i A(\vec{p}, \omega_p) + B(\vec{p}, \omega_p)]^{-1}, \quad (2.1)$$

with vector and scalar quark dressing functions  $C, A, B$ . At physical, antiperiodic boundary conditions the corresponding Matsubara frequencies are given by  $\omega_p(n_t) = (2\pi T)(n_t + 1/2)$ . The ordinary quark condensate can be extracted from the trace of the quark propagator by

$$\langle \bar{\psi} \psi \rangle_\varphi = Z_m Z_2 N_c T \sum_{n_t} \int \frac{d^3 p}{(2\pi)^3} \text{tr}_D S(\vec{p}, \omega_p). \quad (2.2)$$

For vanishing bare quark masses this integral is well-behaved and delivers the chiral condensate, whereas at finite bare quark masses it is quadratically divergent and needs to be properly regularized.

Consider now non-standard,  $U(1)$ -valued boundary conditions in the temporal direction established by the equation  $\psi(\vec{x}, 1/T) = e^{i\varphi} \psi(\vec{x}, 0)$  for the quark field  $\psi$  with the boundary angle  $\varphi \in [0, 2\pi[$ . For the physical antiperiodic fermion boundary conditions we have  $\varphi = \pi$ , whereas  $\varphi = 0$  corresponds to periodic boundary conditions. The corresponding Matsubara frequencies are given by  $\omega_p(n_t, \varphi) = (2\pi T)(n_t + \varphi/2\pi)$ . In this non-standard framework one can evaluate a quark condensate by

$$\langle \bar{\psi} \psi \rangle_\varphi = Z_2 N_c T \sum_{n_t} \int \frac{d^3 p}{(2\pi)^3} \text{tr}_D S(\vec{p}, \omega_p(\varphi)) \quad (2.3)$$

with the conventional quark condensate obtained for  $\varphi = \pi$  and multiplication with  $Z_m$ . It has been shown in [22] that the Fourier-transform

$$\Sigma_1 = \int_0^{2\pi} \frac{d\varphi}{2\pi} e^{-i\varphi} \langle \bar{\psi} \psi \rangle_\varphi \quad (2.4)$$

of this  $\varphi$ -dependent condensate delivers a quantity that transforms under center transformations exactly like the Polyakov-loop and is therefore an order parameter for the deconfinement transition. This quantity  $\Sigma_1$  is called the dual condensate or dressed Polyakov loop.

The relation of  $\Sigma_1$  to the ordinary Polyakov-loop becomes transparent in the following loop expansion of the  $\varphi$ -dependent condensate:

$$\langle \bar{\psi} \psi \rangle_\varphi = \sum_{l \in \mathcal{L}} \frac{e^{i\varphi n(l)}}{(am)^{|l|}} U(l). \quad (2.5)$$

Here  $\mathcal{L}$  denotes the set of all closed loops  $l$  with length  $|l|$  on a lattice with lattice spacing  $a$ . Furthermore  $m$  is the quark mass.  $U(l)$  stands for the chain of link variables in a loop  $l$  multiplied with appropriate sign and normalization factors, see Ref. [22] for details. Each loop that closes around the temporal boundary picks up factors of  $e^{\pm i\varphi}$  according to its winding number  $n(l)$ . Correspondingly, the Fourier-transform in Eq. (2.4) projects out exactly those loops which wind once around the temporal direction of the lattice (therefore the notation  $\Sigma_1$ ). In the limit of heavy quark masses long loops are suppressed by  $1/m^{|l|}$  and therefore only the straight line along the temporal direction of the lattice survives; the dual condensate is then equal to the ordinary Polyakov-loop.

An interesting property of the dual condensate  $\Sigma_1$  is the fact that it can be evaluated with functional methods [18], as we will see in the following.

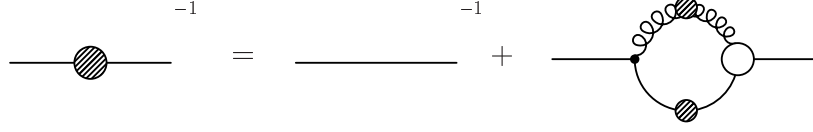


**Figure 1:** The Dyson-Schwinger equation for the quark propagator. Filled circles denote dressed propagators whereas the empty circle stands for the dressed quark-gluon vertex.

### 3. The Dyson-Schwinger equation for the quark propagator at finite temperature

The Dyson-Schwinger equation for the quark propagator Eq. (2.1) is displayed diagrammatically in Fig. 1. At finite temperature  $T$  it is given by

$$S^{-1}(p) = Z_2 S_0^{-1}(p) - C_F Z_{1f} g^2 T \sum_{n_k} \int \frac{d^3 k}{(2\pi)^3} \gamma_\mu S(k) \Gamma_\nu(k, p) D_{\mu\nu}(p - k), \quad (3.1)$$

with  $p = (\vec{p}, \omega_p)$  and  $k = (\vec{k}, \omega_k)$  and renormalization factors  $Z_2$  and  $Z_{1f}$ . Here  $D_{\mu\nu}$  denotes the (transverse) gluon propagator in Landau gauge and  $\Gamma_\nu$  the quark-gluon vertex. The bare quark propagator is given by  $S_0^{-1}(p) = i\gamma \cdot p + m$ . The Casimir factor  $C_F = (N_c^2 - 1)/N_c$  stems from the color trace; here we only consider the gauge group  $SU(2)$ . The quark dressing functions  $A, B, C$  can be extracted from Eq. (3.1) by suitable projections in Dirac-space.

In order to solve this equation we have to specify explicit expressions for the gluon propagator and the quark-gluon vertex. At finite temperatures the tensor structure of the gluon propagator contains two parts, one transversal and one longitudinal to the heat bath. The propagator is then given by ( $q = (\vec{q}, \omega_q)$ )

$$D_{\mu\nu}(q) = \frac{Z_T(q)}{q^2} P_{\mu\nu}^T(q) + \frac{Z_L(q)}{q^2} P_{\mu\nu}^L(q) \quad (3.2)$$

with transverse and longitudinal projectors

$$P_{\mu\nu}^T(q) = \left( \delta_{ij} - \frac{q_i q_j}{\vec{q}^2} \right) \delta_{i\mu} \delta_{j\nu}, \quad P_{\mu\nu}^L(q) = P_{\mu\nu}(q) - P_{\mu\nu}^T(q), \quad (3.3)$$

with  $(i, j = 1 \dots 3)$ . The transverse dressing  $Z_T(\vec{q}, \omega_q)$  is also known as magnetic dressing function of the gluon, whereas the longitudinal component  $Z_L(q)$  is called electric dressing function of the gluon propagator. At zero temperatures Euclidean  $O(4)$ -invariance requires both dressing functions to agree, i.e.  $Z_T(q) = Z_L(q) = Z(q)$ .

The temperature dependence of the gluon propagator can be inferred from recent lattice calculations. The results of Ref. [24] are shown in Fig. 2. The temperature effects on both the magnetic and electric dressing functions are such that there are almost no effects when comparing the  $T = 0$  result with  $T = 119$  MeV. Further increasing the temperature to  $T = 298$  MeV and  $T = 597$  MeV significantly decreases the bump in the magnetic dressing function around  $p^2 = 1$  GeV<sup>2</sup>. There is no indication that this decrease takes special notice of the critical temperature  $T_c \approx 300$  MeV for quenched QCD with gauge group  $SU(2)$ . The opposite seems to be true for the electric part of the propagator. Here from  $T = 119$  MeV to  $T = 300$  MeV one observes a clear increase of the bump

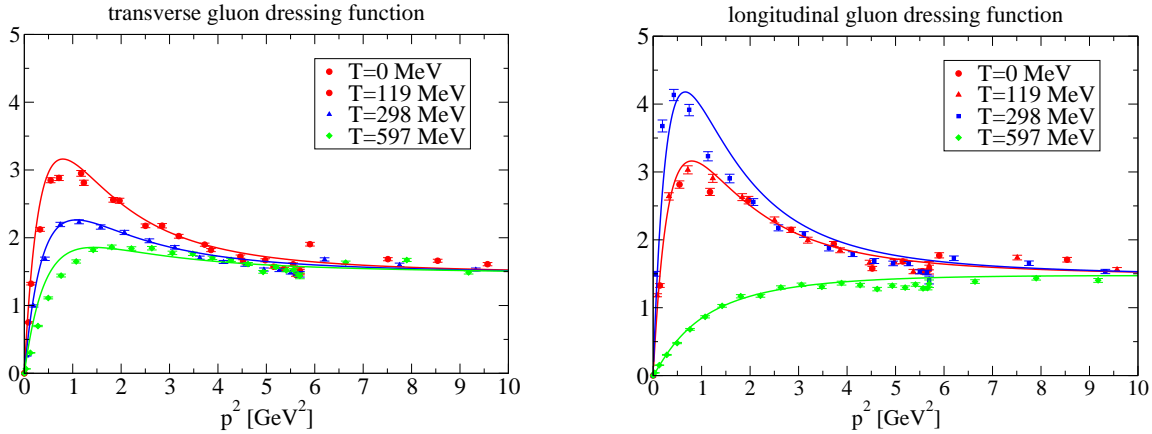


**Figure 2:** Quenched  $SU(2)$  lattice results [24] for the transverse dressing function  $Z_T(q)$  and the longitudinal dressing function  $Z_L(q)$  of the gluon propagator together with the fit functions [18].

in the dressing function  $Z_L(q)$  and a subsequent decrease when the temperature is further raised to  $T = 597$  MeV. Pending further investigation it seems reasonable to assume that the maximum of the bump is reached at or around the critical temperature  $T_c \approx 300$  MeV.

Although the lattice data still have considerable systematic errors [24] they may very well correctly represent the qualitative temperature dependence of the gluon propagator. We therefore use a temperature dependent (qualitative) fit to the data as input into the DSE; this fit is also displayed in Fig. 2 (straight lines). The fit functions are described in detail in Refs. [18, 19] and shall not be repeated here for brevity. Note, however, that we also inherit the scale determined on the lattice using the string tension  $\sqrt{\sigma} = 0.44$  GeV [24].

For the quark-gluon vertex with gluon momentum  $q = (\vec{q}, \omega_q)$  and the quark momenta  $p = (\vec{p}, \omega_p), k = (\vec{k}, \omega_k)$  we employ the following temperature dependent model

$$\Gamma_v(q, k, p) = \tilde{Z}_3 \left( \delta_{4\nu} \gamma_4 \frac{C(k) + C(p)}{2} + \delta_{j\nu} \gamma_j \frac{A(k) + A(p)}{2} \right) \times \left( \frac{d_1}{d_2 + q^2} + \frac{q^2}{\Lambda^2 + q^2} \left( \frac{\beta_0 \alpha(\mu) \ln[q^2/\Lambda^2 + 1]}{4\pi} \right)^{2\delta} \right), \quad (3.4)$$

where  $\delta = -9/44$  is the anomalous dimension of the vertex. The dependence of the vertex on the quark dressing functions  $A$  and  $C$  is motivated by the Slavnov-Taylor identity for the vertex. The remaining fit function is purely phenomenological, see e.g. [25] where an elaborate version of such an ansatz has been used to describe meson observables. The parameters are given by  $d_1 = 7.6 \text{ GeV}^2$  and  $d_2 = 0.5 \text{ GeV}^2$ . A moderate variation of these parameters shifts the critical temperatures of both, the chiral and the deconfinement transition but leaves all qualitative aspects of the results presented below unchanged.

The truncation scheme described above has the merit to explicitly implement a realistic temperature dependence of the gluon propagator and the quark-gluon vertex beyond simple ansätze, see e.g. [14, 12, 26, 27] for previous approaches. The explicit expressions of the resulting DSEs for the quark dressing functions together with the details of our numerical method are given in Ref. [19].

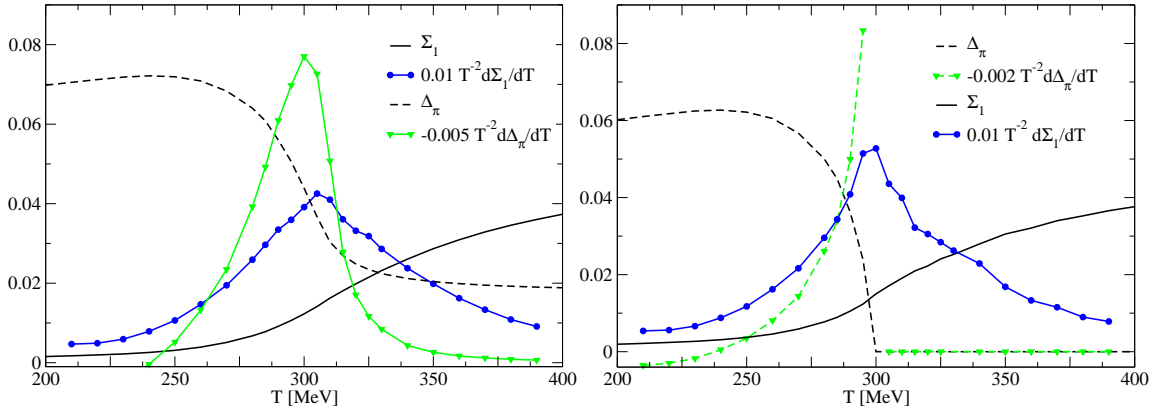


**Figure 3:** Left diagram: Temperature dependence of the dressed Polyakov-loop  $\Sigma_1$  and the conventional quark condensate  $\Delta_\pi \equiv \langle \bar{\psi}\psi \rangle_{\varphi=\pi}$  together with their derivatives for  $m = 10\text{MeV}$ . Right diagram: The same quantities in the chiral limit.

#### 4. Numerical results

In Fig. 3 we display our numerical results for the ordinary and the dual quark condensate together with their (normalized) temperature derivatives once evaluated for a quark mass of  $m = 10\text{MeV}$  and once evaluated in the chiral limit. One clearly sees the difference in the chiral transition: whereas at finite bare quark mass we encounter a crossover the transition changes into a second order phase transition in the chiral limit. In the first case the corresponding temperature derivative shows a peak at  $T_c = 301(2)\text{ MeV}$ , whereas it diverges at  $T_c = 298(1)\text{ MeV}$  in the second case. We also extracted the corresponding transition temperatures from the chiral susceptibility

$$\chi_R = m^2 \frac{\partial}{\partial m} \left( \langle \bar{\psi}\psi \rangle_T - \langle \bar{\psi}\psi \rangle_{T=0} \right). \quad (4.1)$$

The results for quark mass  $m = 10\text{MeV}$  are given in table 1.

The corresponding transition temperature for the deconfinement transition can be read off the dual quark condensate (or dressed Polyakov loop). At finite quark mass and in the chiral limit we observe a distinct rise in the dual condensate around  $T \approx 300\text{ MeV}$ . The corresponding (normalized) temperature derivative shows peaks at  $T_{dec} = 308(2)\text{ MeV}$  for quark mass  $m = 10\text{MeV}$ . In the chiral limit this peak moves to  $T_{dec} = 299(3)\text{ MeV}$ .

In general we note that the chiral and deconfinement transition are close together. There are a few MeV difference between the different transition temperatures for the crossover at finite quark masses, whereas both transitions occur at the same temperature (within errors) in the chiral limit. These findings agree with early expectations from lattice simulations [28].

$T_c$	$T_{\chi_R/T^4}$	$T_{\chi_R}$	$T_{dec}$
301(2)	304(1)	305(1)	308(2)

**Table 1:** Transition temperatures for the chiral and deconfinement transition for quark mass  $m = 10\text{MeV}$ .

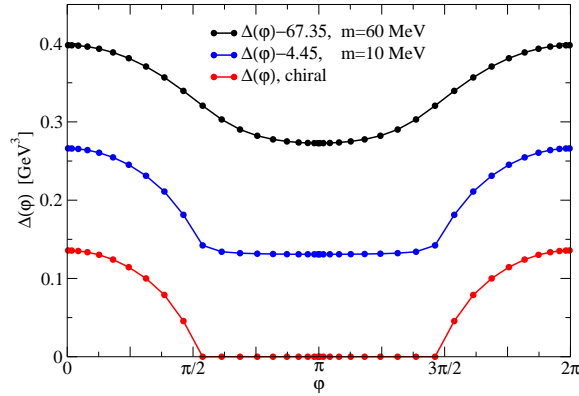


**Figure 4:** Angular dependence of the quark condensate evaluated at two different quark masses and in the chiral limit at  $T = 400$  MeV.

Furthermore we wish to emphasize that the present calculation, although carried out with quenched lattice results for the gluon propagator, is in itself not strictly quenched: our ansatz for the quark-gluon vertex is too simple to strictly represent the quenched theory. This can be seen from the fact that the dressed Polyakov-loop is not strictly zero below the deconfinement transition. Consequently we do not observe the second order deconfinement phase transition expected from quenched  $SU(2)$  Yang-Mills theory. Note, however, that even if our vertex were strictly quenched it is not clear whether the lattice input for the gluon propagator is precise enough to allow for an observation of the second order phase transition.

The details of the mass dependence of the  $\varphi$ -dependent condensate are studied in Fig. 4. We compare the angular dependence of the condensate at  $T = 400$  MeV for two different quark masses and in the chiral limit. We clearly see a broadening in the central dip of the graphs with decreasing quark mass. This can be readily understood from the loop expansion of the quark condensate, Eq.(2.5). At sufficiently large quark masses large loops are suppressed by powers of  $1/m$ . As a result only loops winding once around the torus should contribute in Eq. (2.5) and the resulting angular behavior of the condensate should be proportional to  $\cos(\varphi)$ . Indeed, this is what we see: the result for our largest quark mass can be well fitted by only few terms in an expansion  $\Delta(\varphi) = \sum_{n=0}^N a_n \cos(n\varphi)$  and the first term is by far the largest contribution. For smaller quark masses we observe also sizeable contributions from terms  $\cos(n\varphi)$  with  $n > 1$ . In the plot, these contributions are responsible for the flat area around the antiperiodic boundary angle  $\varphi = \pi$ . Approaching the chiral limit this area becomes flatter and finally develops a derivative discontinuity at two finite values of  $\varphi = \pi \pm L$ . These indicate the breakdown of the loop expansion Eq. (2.5) in the chiral limit.

Finally we show the angular and temperature dependence of the  $\varphi$ -dependent condensate  $\Delta_\varphi(T)$  in Fig. 5. The 3d-plot clearly shows the different evolution of the condensate at varying boundary conditions. Whereas at physical antiperiodic boundary angle  $\varphi = \pi$  we observe the second order chiral phase transition also shown in Fig. 3, we find a monotonically rising condensate at the periodic boundary conditions  $\varphi = 0$ . For larger temperatures (not shown in the plot) we can

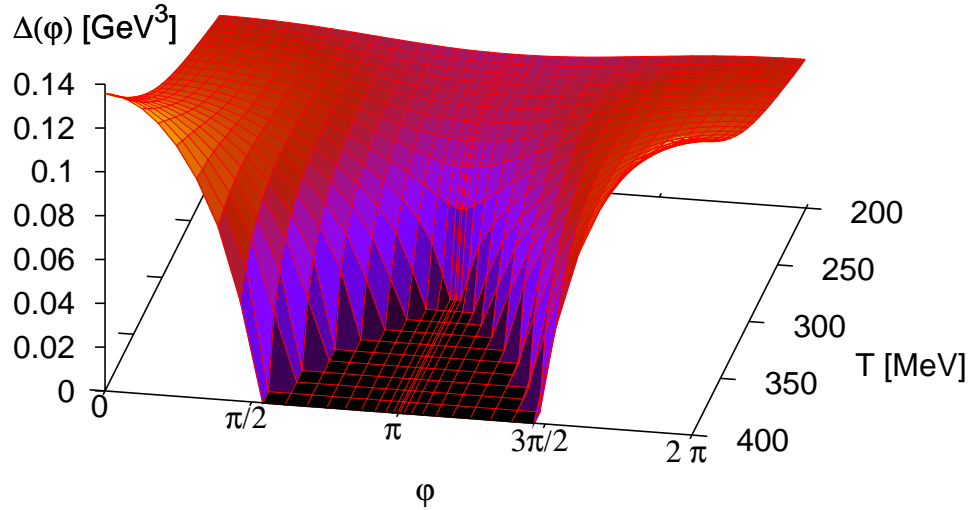


**Figure 5:** A 3d-plot of the angular and temperature dependence of the chiral quark condensate.

extract a quadratic rise of the  $\varphi$ -dependent condensate  $\Delta_{\varphi=0}(T)$ ,

$$\Delta_{\varphi=0}(T) \sim T^2 \quad \text{for } T \gg T_c. \quad (4.2)$$

This behavior can also be extracted analytically from Eqs. (3.1) and (2.2) for the quark propagator and the quark condensate as shown in the appendix of Ref. [19]. Around the physical value of  $\varphi = \pi$  we see a plateau with  $\Delta_{\varphi}(T) = 0$  that gets broader with increasing temperature. The width of this plateau seems to settle at a finite value smaller than  $2\pi$  for  $T > 2T_c$ ; however from the available results we can neither show nor exclude that it approaches  $2\pi$  very slowly for  $T \rightarrow \infty$ .

## 5. Summary

In this talk we addressed the chiral and the deconfinement transition of quenched QCD. We showed results for the order parameter for the chiral transition, the quark condensate, and an order parameter for the deconfinement transition, the dressed Polyakov loop extracted from the Landau gauge quark propagator evaluated at a continuous range of boundary conditions for the quark fields. We found almost coinciding transition temperatures for the chiral and the deconfinement transition at a moderate quark mass of the order of an up-quark. In the chiral limit the two transitions coincide within error. We find a second order chiral phase transition at  $T_{\chi_R}/T^4 = 298(1)$  MeV and a similar temperature for the deconfinement transition,  $T_{dec} = 299(3)$  MeV. It is worth to emphasize



again that both transition temperatures are extracted from the properties of the quark propagator, respectively the underlying properties of the Dirac operator.

The framework used in this work is quenched  $SU(2)$  Yang-Mills theory. Our transition temperature may be translated into the corresponding ones of quenched  $SU(3)$  QCD using the relations  $T_c/\sqrt{\sigma} = 0.709$  ( $SU(2)$ ) and  $T_c/\sqrt{\sigma} = 0.646$  ( $SU(3)$ ) between the respective critical temperatures and the string tension [30]. The resulting transition temperature is then  $T_{\chi_R/T^4} \approx T_{dec} \approx 272$  MeV in the chiral limit. In order to work in the full, unquenched theory we would have to take into account quark-loop effects in the gluon propagator and meson effects in the quark-gluon vertex [25]. These effects will shift the transition temperatures below  $T = 200$  MeV, see [3, 4] for latest results for  $N_f = 2 + 1$  quark flavors. As concerns the dual condensate and scalar dressing function in the unquenched formulation one needs to carefully take into account effects due to the Roberge-Weiss symmetry [29]. This is because of the formal similarity of the continuous boundary conditions for the quark field to an imaginary chemical potential, see [20] for details.

Note: After completion of this proceedings contribution also first results for the dual condensate evaluated in the PNJL-model became available [31].

### Acknowledgments

We thank Falk Bruckmann, Christof Gattringer, Erwin Laermann, Jan Pawłowski, Rob Pisarski, Lorenz von Smekal and Wolfgang Soeldner for discussions. We are grateful to Axel Maas for discussions and for making the lattice data of Ref. [24] available. This work has been supported by the Helmholtz Young Investigator Grant VH-NG-332 and by the Helmholtz Alliance HA216-TUD/EMMI.

### References

- [1] P. de Forcrand and O. Philipsen, JHEP **0701** (2007) 077 [arXiv:hep-lat/0607017]; O. Philipsen, arXiv:0907.4668 [hep-ph].
- [2] L. McLerran and R. D. Pisarski, Nucl. Phys. A **796** (2007) 83 [arXiv:0706.2191 [hep-ph]]; L. McLerran, K. Redlich and C. Sasaki, Nucl. Phys. A **824**, 86 (2009) [arXiv:0812.3585 [hep-ph]].
- [3] A. Bazavov *et al.*, arXiv:0903.4379 [hep-lat].
- [4] Y. Aoki *et al.*, arXiv:0903.4155 [hep-lat].
- [5] S. Ejiri, C. R. Allton, S. J. Hands, O. Kaczmarek, F. Karsch, E. Laermann and C. Schmidt, Prog. Theor. Phys. Suppl. **153** (2004) 118 [arXiv:hep-lat/0312006].
- [6] B. J. Schaefer, these proceedings; F. Karsch, B. J. Schaefer, M. Wagner, J. Wambach, in preparation.
- [7] B. J. Schaefer, J. M. Pawłowski and J. Wambach, Phys. Rev. D **76**, 074023 (2007) [arXiv:0704.3234 [hep-ph]].
- [8] S. Roessner, T. Hell, C. Ratti and W. Weise, Nucl. Phys. A **814** (2008) 118 [arXiv:0712.3152 [hep-ph]].
- [9] K. Fukushima, Phys. Rev. D **78** (2008) 114019 [arXiv:0809.3080 [hep-ph]].
- [10] M. A. Stephanov, PoS **LAT2006** (2006) 024 [arXiv:hep-lat/0701002].
- [11] J. Berges, N. Tetradis and C. Wetterich, Phys. Rept. **363**, 223 (2002) [arXiv:hep-ph/0005122]; H. Gies, arXiv:hep-ph/0611146.

- [12] C. D. Roberts and S. M. Schmidt, *Prog. Part. Nucl. Phys.* **45**, S1 (2000), [arXiv:nucl-th/0005064].
- [13] C. S. Fischer, *J. Phys. G* **32**, R253 (2006) [arXiv:hep-ph/0605173].
- [14] A. Bender, D. Blaschke, Y. Kalinovsky and C. D. Roberts, *Phys. Rev. Lett.* **77** (1996) 3724, [arXiv:nucl-th/9606006].
- [15] J. Braun and H. Gies, *JHEP* **0606**, 024 (2006) [arXiv:hep-ph/0602226].
- [16] J. Braun, H. Gies and J. M. Pawłowski, arXiv:0708.2413 [hep-th]; F. Marhauser and J. M. Pawłowski, arXiv:0812.1144 [hep-ph].
- [17] J. Braun, arXiv:0810.1727 [hep-ph].
- [18] C. S. Fischer, *Phys. Rev. Lett.* **103**, 052003 (2009), arXiv:0904.2700 [hep-ph].
- [19] Christian S. Fischer and Jens A. Mueller, arXiv:0908.0007 [hep-ph].
- [20] J. Braun, L. Haas, F. Marhauser and J. M. Pawłowski, arXiv:0908.0008 [hep-ph].
- [21] C. Gattringer, *Phys. Rev. Lett.* **97** (2006) 032003, [arXiv:hep-lat/0605018].
- [22] E. Bilgici, F. Bruckmann, C. Gattringer and C. Hagen, *Phys. Rev. D* **77** (2008) 094007, [arXiv:0801.4051].
- [23] F. Synatschke, A. Wipf and K. Langfeld, *Phys. Rev. D* **77** (2008) 114018, [arXiv:0803.0271 [hep-lat]].
- [24] A. Cucchieri, A. Maas and T. Mendes, *Phys. Rev. D* **75**, 076003 (2007), [arXiv:hep-lat/0702022].
- [25] C. S. Fischer and R. Williams, *Phys. Rev. D* **78** (2008) 074006, [arXiv:0808.3372 [hep-ph]].
- [26] P. Maris, C. D. Roberts, S. M. Schmidt and P. C. Tandy, *Phys. Rev. C* **63**, 025202 (2001) [arXiv:nucl-th/0001064].
- [27] D. Horvatic, D. Klabucar and A. E. Radzhabov, *Phys. Rev. D* **76** (2007) 096009 [arXiv:0708.1260 [hep-ph]].
- [28] F. Karsch, arXiv:hep-lat/9903031.
- [29] A. Roberge and N. Weiss, *Nucl. Phys. B* **275** (1986) 734.
- [30] J. Fingberg, U. M. Heller and F. Karsch, *Nucl. Phys. B* **392** (1993) 493; [arXiv:hep-lat/9208012].  
O. Kaczmarek, F. Karsch, P. Petreczky and F. Zantow, *Phys. Lett. B* **543** (2002) 41; [arXiv:hep-lat/0207002].  
B. Lucini, M. Teper and U. Wenger, *JHEP* **0502** (2005) 033; [arXiv:hep-lat/0502003].
- [31] K. Kashiwa, H. Kouno and M. Yahiro, arXiv:0908.1213 [hep-ph].